COMMUNICATIONS CHEMISTRY

ARTICLE

DOI: 10.1038/s42004-018-0055-6 OPEN

Negative fluorescence anisotropy of phosphole oxide-based dyes in nematic liquid crystals

Takuya Ohzono [1], Tetsuo Yatabe[2], Chenguang Wang[3], Aiko Fukazawa [4] & Shigehiro Yamaguchi[3,4]

It is important to understand how solute molecules align in anisotropic media such as liquid crystals and biological membranes. Alignment of fluorescent probes used in polarised fluorescence microscopy is of interest because anisotropy of the medium is indirectly estimated through the fluorescence intensity originating from the transition dipole moments fixed on the molecule. Here we report fluorescence anisotropies of a series of phosphole oxide-based dyes with an elongated π-conjugated system, along which the transition dipole moment lies, in nematic liquid crystals. We observe that as the number, size and rigidity of substituents protruding from the π-conjugated plane increase, the transition dipole moment tends to tilt away from the nematic director over the magic angle, ~54.7°, showing conspicuous negative fluorescence anisotropy. Analysis of molecular shapes suggests that the substitutions modulate the interaction with the nematic mean field, impacting the direction of the principal molecular axis aligned with the nematic director.

[1] Electronics and Photonics Research Institute, National Institute of Advanced Industrial Science and Technology, (AIST) 1-1-1 Higashi, Tsukuba 305-8565, Japan. [2] Interdisciplinary Research Center for Catalytic Chemistry, AIST, 1-1-1 Higashi, Tsukuba 305-8565, Japan. [3] Institute of Transformative Bio-Molecules (ITbM), Nagoya University, Furo, NagoyaChikusa 464-8602, Japan. [4] Department of Chemistry, Graduate School of Science, and Integrated Research Consortium on Chemical Sciences (IRCCS), Nagoya University, Furo, NagoyaChikusa 464-8602, Japan. Correspondence and requests for materials should be addressed to T.O. (email: ohzono-takuya@aist.go.jp)

Liquid crystals[1–4] and other anisotropic forms of soft matter, such as biological membranes[5], exhibit unique functions owing to their anisotropic properties with their tunability, such as electrically switchable optical shutters for display applications and the anisotropic nature of functional bio-molecules in flexible membranes. To clarify how they induce these functions, the characterisation of the spatial distribution of the anisotropic states is critical. One of the simplest and most powerful tools for this purpose is polarised optical microscopy (POM), which adds the spatial distribution of optical anisotropy (or birefringence) related to the local anisotropic states. In addition, fluorescence POM (FPOM)[6–8], using fluorescence probes (or directly observing the fluorescence of the constituent molecules)[9,10], has also been an important method to directly observe the distribution of anisotropy. Both microscopies have long become necessary, especially in liquid crystals and biological research.

Dye-doped nematic liquid crystals (NLCs) can exhibit fluorescence anisotropy. NLC is the simplest non-trivial phase of liquid crystals to possess long-range orientational order and no positional order, commonly characterised by a unit vector $\boldsymbol{n}$ known as the director. Depending on the imposed boundary conditions, NLCs have known to form various three-dimensional distributions of $\boldsymbol{n}$ and are often accompanied by topological defects[3,4,11]. The defects have been drawing attention as tuneable or reconfigurable templates for nano-/micro-patterning of small non-LC objects, eg, micro particles[12–18], polymers[19], self-assembled molecules[20,21] and low-molecular-weight solutes[22,23]. Thus, characterisation of local non-uniform distributions of $\boldsymbol{n}$, eg, around the defects, has increasingly become important, where FPOM (including confocal type[24–26]) with probes possessing proper fluorescence anisotropy has been a powerful method.

Studies of probe dyes and other guest molecules, including fluorescent dyes in host media including NLCs,[27] were conducted intensively at the end of 20th century, with an intention of applying them to a display application, namely guest–host mode displays[28–33]. Most research emphasised the dyes with strong positive anisotropy of absorption, or rarely, fluorescence, which shows stronger absorption or emission of light in the direction parallel to $\boldsymbol{n}$ in comparison to that in the perpendicular direction, because of the merits in improving the contrast of guest–host mode displays. Moreover, for FPOM of NLC dyes with strong positive fluorescence anisotropy, such as perylenedicarboximide[24–26,34], dyes with positive anisotropy have been used to acquire better contrast and understanding of alignment of NLC molecules. However, little has been reported regarding dyes with negative anisotropy[35–37], especially those with fluorescence[38].

Recently the negative anisotropy of a phosphole oxide-based dye, C-Naphox[39], in NLC was reported[40]. Since this dye has a high photobleaching resistance, the detailed FPOM study of NLC defects has become possible, eg, uncovering their three-dimensional structures being based on alignment information complementary to that given by the dyes with positive anisotropy. This example demonstrates a new use of fluorescence dyes with negative anisotropy besides guest–host mode displays. In light of these findings, the development of new dyes with enhanced negative fluorescence anisotropy, which improve the FPOM contrast, should be important to further increase of the utility of this methodology. However, there is no principle for the molecular design of such dyes at present because the origin of the negative anisotropy of the phosphole oxide-based dye remains unclear.

In general, the observed fluorescence anisotropy originates from the statistically anisotropic orientational distribution of transition dipole moments (TDMs), oscillators, for light absorption and emission, which are vectors generally fixed to the molecular framework. In other words, only the second-order moment of the orientational distribution function of TDMs is experimentally detected. The anisotropic distribution of TDMs is closely related to that of dye molecules that align with $\boldsymbol{n}$ feeling the nematic mean field potential. In general, there should be a specific axis, often called the long axis (LX), of the dye molecule that statistically coincides with $\boldsymbol{n}$. When dyes with strong positive anisotropy are considered, it is reasonable to assume that LX coincides with the TDM direction, which has been applied in many studies of positive anisotropic dyes for guest–host mode applications. In this specific case, the principle for the molecular design to obtain strong anisotropy becomes simple; the elongated and rigid shape is preferred to render TDM parallel to $\boldsymbol{n}$ with a narrow distribution. However, when negative anisotropy is considered, the TDM will never be parallel to LX. Therefore, the experiments only give the degree of anisotropic distribution of TDMs, which statistically tilt away from $\boldsymbol{n}$ over the magic angle, ~54.7° and no information regarding LX. Thus, the relation between the fluorescence anisotropy and molecular structure is missing in general.

One of the ways to discuss this relation is to rely on theoretical and computational methods. Ferrarini et al. reported[41–43] that the LX of a solute molecule in an NLC and the second-order parameter tensor can be tolerably estimated from the molecular surface[44,45]. The molecular surface used for the analysis can be obtained separately through geometry optimisation based on quantum chemical (QC) calculations. The TDM vector on the molecular framework can be also estimated from the optimised

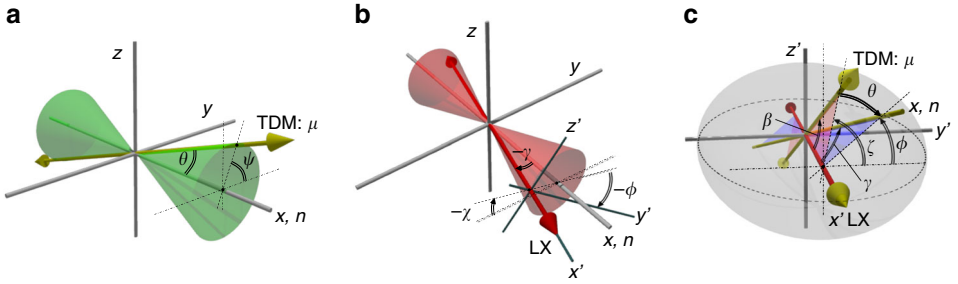

Fig. 1 Coordinate systems. **a** TDM unit vector $\boldsymbol{\mu}$ of a dye molecule on the laboratory coordinate is expressed as $\boldsymbol{\mu} = (\cos\theta, \sin\theta\cos\psi, \sin\theta\sin\psi)$. The nematic director $\boldsymbol{n}$ is set parallel to the *x*-axis, (1, 0, 0). The distribution of angle ψ is homogeneous due to the symmetry of the uniaxial nematic, which is represented by the green cones. The excitation and collected fluorescence light waves propagate along the *z*-axis on microscopies. **b** Relation between the laboratory (*x*, *y*, *z*) and molecular coordinates (*x*′, *y*′, *z*′). The long molecular axis, LX, of the dye, which aligns along $\boldsymbol{n}$ on the statistical average, is chosen as the *x*′-axis. LX can be estimated by the molecular shape analysis. The distribution of angle χ is homogeneous due to the symmetry of the uniaxial nematic, which is represented by the red cones. **c** The TDM vector $\boldsymbol{\mu}$ on the molecular coordinate is expressed as $\boldsymbol{\mu} = (\cos\beta, \sin\beta\cos\zeta, \sin\beta\sin\zeta)$. The *z*′-axis can be chosen as the shortest molecular axis, which can also be estimated by the molecular shape analysis providing a rough estimate of the molecular shape shown by the grey ellipsoid

geometries in the ground and excited states, with the wave functions based on the Frank–Condon principle. Consequently, it is possible to computationally estimate the experimentally observed fluorescence (and absorption) anisotropy. Since the apparent molecular structures are treated, this approach would be helpful to discuss the correlation between the negative anisotropy and the difference in molecular structures.

Here, with the aid of such theoretical analysis, we investigate steady-state fluorescence anisotropy of a series of phosphole oxide-based dyes[39,46–48] in NLCs to clarify the relation between the experimentally observed negative anisotropy and the molecular structures. In addition, the theoretically derived general principle of the molecular design of dyes for controlling the fluorescence anisotropy and molecular alignment in NLCs, as well as conditions for realising strong negative anisotropy, is discussed.

Results

Coordinate system. The present laboratory (x, y, z) and molecular (x', y', z') coordinate systems are shown in Fig. 1. A thin planar cell with $\boldsymbol{n}$ set parallel to the x-axis are investigated using FPOM with the optical axis along the z-axis (Fig. 1a). A dye molecule fluctuates in the NLC and the coordinate fixed to the molecular framework (x', y', z') is expressed on the laboratory coordinate by using the Euler angles (ϕ, γ, χ) shown in Fig. 1b. The basal unit vectors of the molecular coordinate on the laboratory one are expressed as $\boldsymbol{x}' = (\cos\gamma, -\cos\chi\sin\gamma, \sin\chi\sin\gamma)$, $\boldsymbol{y}' = (\sin\gamma\cos\phi, \cos\chi\cos\gamma\cos\phi - \sin\chi\sin\phi, -\sin\chi\cos\gamma\cos\phi - \cos\chi\sin\phi)$ and $\boldsymbol{z}' = (\sin\gamma\sin\phi, \cos\chi\cos\gamma\sin\phi - \sin\chi\cos\phi, -\sin\chi\cos\gamma\sin\phi - \cos\chi\cos\phi)$, ie, $\boldsymbol{e}_{x,y,z} = R_x(-\chi)R_z(-\gamma)R_x(-\phi)\boldsymbol{e}_{x,y,z}$, where $R_i(q)$ is the rotation matrix with respect to the i-axis by angle q.

The TDM vector expressed as $\boldsymbol{\mu} = (\cos\beta, \sin\beta\cos\zeta, \sin\beta\sin\zeta)$ is fixed on the molecular framework, ie, molecular coordinates, with the two angles (β, ζ) and $\boldsymbol{n}$ (corresponding to the x-axis of the laboratory coordinate) is expressed with two variable angles (γ, ϕ), as shown in Fig. 1c. The basal unit vector of the x-axis, ie, $\boldsymbol{n}$, on the molecular coordinate is expressed as $\boldsymbol{n} = (\cos\gamma, \sin\gamma\cos\phi, \sin\gamma\sin\phi)$. Thus, we have the relation $\boldsymbol{\mu}\cdot\boldsymbol{n} = \cos\theta$.

Dichroic ratio and order parameter of transition dipole moment. The experimentally obtained polarised components of fluorescence intensity under natural (unpolarised) excited light in parallel, $I_{\parallel}$, and perpendicular directions, $I_{\perp}$, to $\boldsymbol{n}$ are related to the dichroic ratio, $R = I_{\parallel}/I_{\perp}$, and to the second moment of the orientational distribution function, $F(\cos\theta)$, of the TDM vector of fluorescence $S_{\mathrm{TDM}} = \langle P_2(\cos\theta)\rangle = (R-1)/(R+2)$, where θ is the angle between the TDM and x-axis (Fig. 1a), $\langle\rangle$ means the statistical average, and P_2 is the second Legendre polynomial (see Supplementary Note 1 for derivation including the case of using polarised light for excitation and the similar relation for the absorption anisotropy measurements).

Expansion of order parameter of TDM using angles on the molecular coordinate. To discuss the relation between S_{TDM} and the molecular structure, S_{TDM} is expanded by angles (γ,ϕ) and (β, ζ) on the molecular coordinate shown in Fig. 1c, using the spherical harmonic addition theorem and the uniaxial nematic symmetry of the system, as

$$S_{\mathrm{TDM}} = S_\beta S_{\mathrm{LX}} + \frac{1}{3}D_{\beta\zeta}D_{\mathrm{LX}} \tag{1}$$

where $S_\beta = \langle P_2(\cos\beta)\rangle = P_2(\cos\beta)$, $S_{\mathrm{LX}} = \langle P_2(\cos\gamma)\rangle$, $D_{\beta\zeta} = \frac{3}{2}\langle\sin^2\beta\cos 2\zeta\rangle = \frac{3}{2}\sin^2\beta\cos 2\zeta$ and $D_{\mathrm{LX}} = \frac{3}{2}\langle\sin^2\gamma\cos 2\phi\rangle$. See Supplementary Note 2 for the derivation. S_β and $D_{\beta\zeta}$ are the unique parameters determined by the angles (β,ζ), which characterise the relative orientation of TDM to LX. S_{LX} is the order parameter of LX of the dye molecule, which characterises the statistical deviation of the LX vector from the nematic director. The special value of β~54.7°, which is often called the magic angle for uniaxially anisotropic systems characterised by the second-order tensor in three dimensions, gives $S_\beta = 0$. D_{LX} characterises the statistical deviation from the molecular rotational symmetry when $\gamma\neq 0$, and is known as flatness (or biaxiality)-order parameter of the dye molecule[1,2].

Equation (1) is used to discuss what and how the factors, ie, four components, associated with the dye molecules affect the experimentally observed S_{TDM}. Moreover, Eq. (1) can provide a guiding principle in designing the molecular structure to tune the value of S_{TDM}. Here, since the components on the right side of Eq. (1) are unavailable from the present experiments, they are computationally estimated from the molecular shape analysis, as shown below.

Molecular shape evaluation using molecular surface tensor. In general, it is difficult to estimate the LX vector, which statistically aligns along $\boldsymbol{n}$, of the dye molecules, especially with a non-rod shape, in an NLC medium from their chemical formulae. Nevertheless, some elegant methods have been proposed[41–44,49–51] and recently investigated with molecular dynamics simulations conducted by Sims et al.[45], showing that the reliable method is based on the evaluation of the solvent-accessible surface of the dye molecule[41,42], which is obtained using QC calculations. The simplest statistical anisotropy of the molecular surface elements can be characterised by evaluating the sum of the second-order tensor product of the unit normal vector $\boldsymbol{t}$ with an outward direction of the surface element ds over the surface. The derivation is similar that of the tensor-order parameter for nematics[1,2]. Here, the tensor $\mathbf{T}$ is defined as

$$\mathbf{T} = \int_s \boldsymbol{t}\otimes\boldsymbol{t}\,\mathrm{d}s, \tag{2}$$

where the integral is conducted over the molecular surface s. The symmetric tensor can be diagonalized to find principal directions, which correspond to the set of eigenvectors orthogonal to each other. Since we may choose the eigenvectors as the molecular coordinates (Fig. 1c), here we particularly set the eigenvector with the smaller, middle, or larger eigenvalue as x', y', or z', respectively. On the molecular coordinate, whose coordinate axes coincide with the principal tensor axes, the tensor has the form of $\mathbf{T} = \begin{pmatrix}\lambda_x & 0 & 0\\ 0 & \lambda_y & 0\\ 0 & 0 & \lambda_z\end{pmatrix}$, where $0 \le \lambda_x \le \lambda_y \le \lambda_z$, $\mathrm{Tr}(\mathbf{T}) = \lambda_x + \lambda_y + \lambda_z = \int_s \mathrm{d}s = A$, and A is the total surface area. $\lambda_i (i = x, y, z)$ physically corresponds to the effective surface area with the normal vector parallel to each principal i'-axis, and thus, $\left(\lambda_x, \lambda_y, \lambda_z\right)$ contains information on the degree of anisotropy of the molecular shape. As indexical values for the anisotropy of the molecular shape, we define

$$(\lambda_S, \lambda_D) = \left(-\left\{\lambda_x - \frac{1}{2}\left[\lambda_y + \lambda_z\right]\right\}, -\left\{\lambda_y - \lambda_z\right\}\right), \tag{3}$$

where a larger λ_S or λ_D means a more elongated or flatter shape. Two extreme cases are expressed with $0 \approx \lambda_x \ll \lambda_y \approx \lambda_z$ and $\lambda_x \approx \lambda_y \approx \lambda_z$, which correspond to the rod with $(\lambda_S, \lambda_D)/A \approx (1, 0)$ and sphere with $(\lambda_S, \lambda_D)/A \approx (0, 0)$, respectively. On this particular molecular coordinate (Fig. 1c), the LX vector is defined and found as the unit vector parallel to the x'-axis. Since the TDM

vector is known from the QC calculation, angles (B,ζ), which indicate the relation between the TDM and LX vectors, are determined, and thus, S_β and $D_{\beta\zeta}$ are calculated.

Estimation of S_{LX} and D_{LX} using simulated molecular shape. Here, the remaining S_{LX} and D_{LX} are derived from the second-order tensor-order parameter of the dye molecules **Q**. Once we obtain the molecular surface, ie, a set of $\boldsymbol{t}$ over the surface, the interaction potential between the molecular surface and the nematic mean field, which has Maier–Saupe type, can be estimated as

$$U(\boldsymbol{n}) = k_B T\varepsilon \int_s P_2(\boldsymbol{n}\cdot\boldsymbol{t})\mathrm{d}s, \tag{4}$$

where $\boldsymbol{n} = \left(n_x, n_y, n_z\right) = (\cos\gamma, \sin\gamma\cos\phi, \sin\gamma\sin\phi)$ is the nematic director on the molecular coordinate (Fig. 1c), k_B is the Boltzmann constant, T is temperature and the positive constant ε is the system-dependent interaction parameter with unit of L^{-2}; in addition, a dilute solute condition is assumed. ε is a function of temperature, and reflects all interactions between NLC and the solute, eg, dipole–dipole interaction and hydrogen bond. The molecular shape affects the integral part through $\boldsymbol{t}$[41].

Since the molecular coordinate has been chosen as eigenvectors of **T** in the previous section, $U(\boldsymbol{n})$ can be simplified as follows. The integral part in Eq. (4) is calculated as

$$\int_s P_2(\boldsymbol{n}\cdot\boldsymbol{t})\mathrm{d}s = \frac{3}{2}\int_s (\boldsymbol{n}\cdot\boldsymbol{t})^2\mathrm{d}s - \frac{A}{2}.$$

The integral part on the right side of this equation is calculated as

$$\int_s (\boldsymbol{n}\cdot\boldsymbol{t})^2\mathrm{d}s = \int_s \left(n_x n_x t_x t_x + n_y n_y t_y t_y + n_z n_z t_z t_z + 2n_x n_y t_x t_y + 2n_y n_z t_y t_z + 2n_z n_x t_z t_x\right)\mathrm{d}s.$$

Since the molecular coordinate is chosen as the eigenvectors of tensor **T**, the molecular shape evaluation using the molecular surface tensor,

$$\int_s \left(t_x t_x, t_y t_y, t_z t_z\right)\mathrm{d}s = \left(T_{xx}, T_{yy}, T_{zz}\right) = \left(\lambda_x, \lambda_y, \lambda_z\right)$$

and

$$\int_s \left(t_x t_y, t_y t_z, t_z t_x\right)\mathrm{d}s = \left(T_{xy}, T_{yz}, T_{zx}\right) = (0,0,0)$$

leading

$$\int_s (\boldsymbol{n}\cdot\boldsymbol{t})^2\mathrm{d}s = n_x n_x\lambda_x + n_y n_y\lambda_y + n_z n_z\lambda_z.$$

Then,

$$\begin{aligned}\int_s P_2(\boldsymbol{n}\cdot\boldsymbol{t})\mathrm{d}s &= \tfrac{3}{2}\left(n_x n_x\lambda_x + n_y n_y\lambda_y + n_z n_z\lambda_z\right) - \tfrac{\lambda_x+\lambda_y+\lambda_z}{2} \\ &= \tfrac{\lambda_x}{2}\left(3n_x^2-1\right) + \tfrac{\lambda_y}{2}\left(3n_y^2-1\right) + \tfrac{\lambda_z}{2}\left(3n_z^2-1\right) \\ &= \left\{P_2(n_x), P_2\left(n_y\right), P_2(n_z)\right\}\cdot\left\{\lambda_x,\lambda_y,\lambda_z\right\}\end{aligned},$$

finally leading

$$\begin{aligned}U(\boldsymbol{n}) &= k_B T\varepsilon\left\{P_2(n_x), P_2\left(n_y\right), P_2(n_z)\right\}\cdot\left\{\lambda_x,\lambda_y,\lambda_z\right\} \\ &= k_B T\varepsilon\left[\frac{3}{2}\boldsymbol{n}_d\cdot\boldsymbol{\lambda} - \frac{A}{2}\right],\end{aligned} \tag{5}$$

where $\boldsymbol{n}_d$ and $\boldsymbol{\lambda}$ are vectors composed of the diagonal components of the tensors $\boldsymbol{n}\otimes\boldsymbol{n}$ and **T**, respectively. It is noted that $U(\boldsymbol{n})$ is minimised with $\boldsymbol{n}$ parallel to the x'-axis, ie, $\boldsymbol{n}_d = (1,0,0)$, because in the direction, the molecule has the lowest effective area, λ_x; $U_{\min} = k_B T\varepsilon\left[\frac{3}{2}\lambda_x - \frac{A}{2}\right]$.

Using Eq. (5), the distribution function $F(\gamma,\phi)$ for $\boldsymbol{n}$ on the molecular coordinate is expressed as a Boltzmann (or Gibbs) distribution:

$$F(\gamma,\phi) = [\exp(-U(\boldsymbol{n})/k_B T)]/Z, \tag{6}$$

where $Z = \int_0^\pi\int_0^{2\pi}\exp(-U(\boldsymbol{n})/k_B T)\sin\gamma\mathrm{d}\gamma\mathrm{d}\phi$ is the normalisation factor, ie, the partition function.

Since the tensor-order parameter **Q** is defined as[1,2]

$$\mathbf{Q} = \langle\mathbf{S}\rangle = \frac{3}{2}\left(\langle\boldsymbol{n}\otimes\boldsymbol{n}\rangle - \frac{\mathbf{E}}{3}\right), \tag{7}$$

where **E** is the unit tensor with $E_{ij} = \delta_{ij}$, δ_{ij} is the Kronecker delta and **S** is known as the Saupe ordering matrix[1,2],

$$\mathbf{S} = \frac{3}{2}\left(\boldsymbol{n}\otimes\boldsymbol{n} - \frac{\mathbf{E}}{3}\right) \tag{8}$$

and is also expressed as

$$\mathbf{Q} = \frac{1}{Z}\int_0^\pi\int_0^{2\pi}\mathbf{S}\exp(-U(\boldsymbol{n})/k_B T)\sin\gamma\mathrm{d}\gamma\mathrm{d}\phi. \tag{9}$$

This is numerically calculated with a certain ε. Finally, S_{LX} and D_{LX}, which are two scalar order parameters of the dye molecule, are derived as

$$S_{LX} = Q_{xx} = \frac{3}{2}\left\langle n_x n_x - \frac{1}{3}\right\rangle, \tag{10}$$

$$D_{LX} = Q_{yy} - Q_{zz} = \frac{3}{2}\left\langle n_y n_y - n_z n_z\right\rangle. \tag{11}$$

Finally, we can simulate S_{TDM} (Eq. (1)) using values of S_β, $D_{\beta\zeta}$, S_{LX} and D_{LX} for each dye molecule in a nematic phase.

Fluorescence and absorption anisotropies of dyes in NLCs. Fluorescence anisotropies of dyes (see Methods and Supplementary Table 1) in several NLCs with different polarities were measured, which are shown in Fig. 2 as order parameters of TDM for fluorescence, $S_{TDM} = \frac{R-1}{R+2}$. It is clear from the data that the S_{TDM} of two reference dyes, C5T and PMN, are relatively higher and positive, indicating positive fluorescence anisotropy utilised in common fluorescence optical microscopy (FOM) studies of NLCs[22]. On the other hand, those for phosphole oxide-based dyes vary from positive to negative depending on the difference in the substituents attached to the π-conjugated plane, which is the main framework of the present dyes and highlighted with green in Fig. 2b. Non-negligible effects of the polarity of NLCs on S_{TDM} of each dye appear, eg, S_{TDM} observed in 5CB show lower values than those in PTTP and MBBA, except for the case of C5T. However, they are small in comparison to those of the difference between dyes. This suggests, though it may be well known from

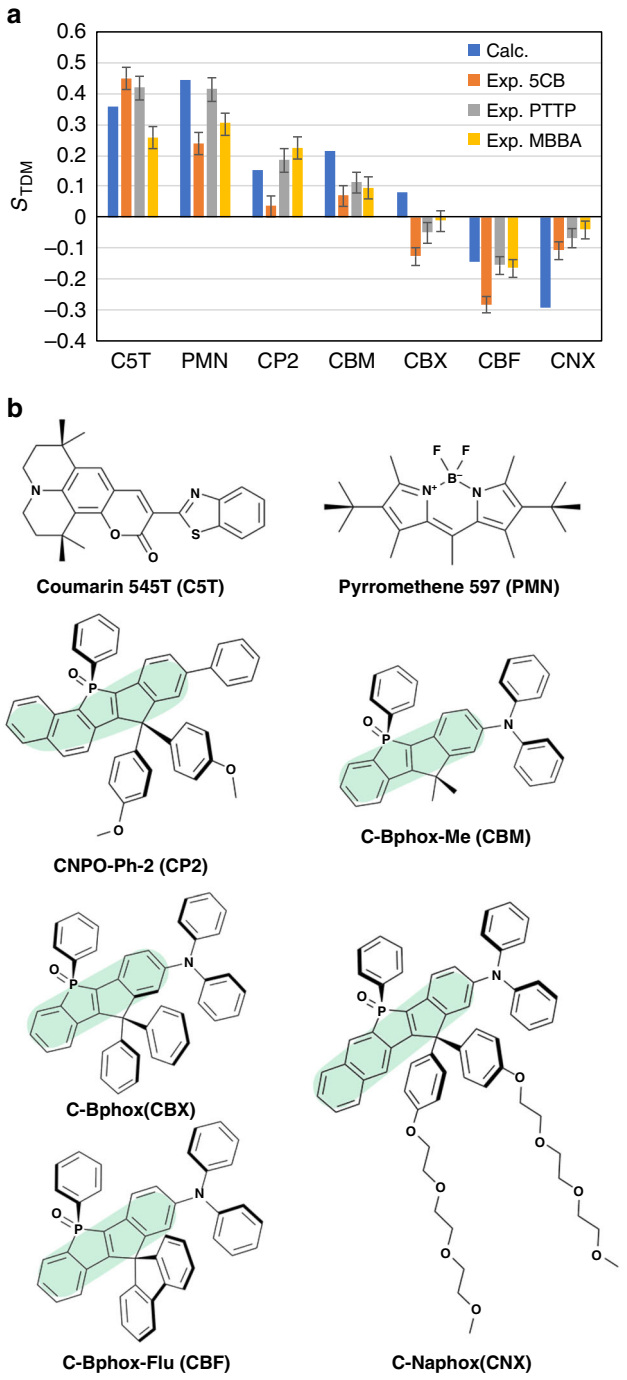

Fig. 2 Fluorescence anisotropy of dyes. **a** Order parameters, S_{TDM}, of fluorescence TDM, which correspond to the fluorescence anisotropy $(R-1)/(R+2) = (I_{\parallel} - I_{\perp})/(I_{\parallel} + 2I_{\perp})$, where $I_{\parallel}$ and $I_{\perp}$ are fluorescence intensities with the analysing polariser parallel and perpendicular to the nematic director $\boldsymbol{n}$, respectively, and R is the fluorescence dichroic ratio, $I_{\parallel}/I_{\perp}$. The bars and their errors show the means and standard deviations of collected fluorescence intensity. The values obtained by theoretical calculations with the interaction parameter $\varepsilon = 0.03$ Å^{-2} are shown with the experimental values obtained with three NLCs—5CB, PTTP and MBBA. **b** Chemical structures of seven fluorescent dyes with abbreviations of their chemical names. Common π-conjugated planes of the phosphole oxide-based dyes are coloured in green

the related studies on solutes in NLCs, that the interaction between a dye and the mean nematic field rather than the specific interaction between the dye and NLC molecules, such as dipole–dipole interactions, is the primary factor governing the alignment state of dyes.

Separately obtained order parameters of the TDM for absorption $S_{TDM\text{-}Abs}$ (Supplementary Figure 1) show a similar tendency with that of fluorescence (Fig. 2a). Note that the values of $S_{TDM\text{-}Abs}$ for the phosphole oxide-based dyes exhibit slight shifts to the positive side with respect to S_{TDM}. The difference between S_{TDM} and $S_{TDM\text{-}Abs}$ generally indicates the discordance between distributions of TDM vectors for fluorescence and absorption. Therefore, although the effect is small, the phosphole oxide-based dyes should have a specific reason for this character, which might be associated with the difference in the structures and/or effective molecular shapes at ground S_0 and excited S_1 states.

According to the theoretical relation shown by Supplementary Equations 1–23 in Supplementary Note 1, the fluorescence dichroic ratio with the polarised excitation light becomes $R_{pol-ex} = R_a \cdot R$. The enhancement of dichroic ratio, which affects the fluorescence contrast of images, for C5T was indeed observed (Supplementary Figure 2) because its $S_{TDM\text{-}Abs}$ is relatively large and positive, ie, $R_a > 1$. However, for CBX and CNX, their $S_{TDM\text{-}Abs}$ close to zero, ie, $R_a \approx 1$, causes little difference between $R_{pol\text{-}ex}$ and R (Supplementary Figure 2).

The effects of the substituents of the phosphole oxide-based dyes on the fluorescence anisotropy are significant and of primary importance in the present study (Fig. 2a). CP2, which has a phenyl group instead of diphenylamino (NPh_2) group found in other compounds, shows weak positive S_{TDM}. CBM, of which two methyl groups on the five-membered ring in the π-conjugated system are smaller in the effective volume than those in other compounds, also shows weak positive S_{TDM}. In contrast, CBX, which has both the NPh_2 group and two phenyl groups at the terminal position and on the five-membered ring, respectively, shows weak negative values of S_{TDM}. Moreover, CBF, which is composed of a rigid fluorene moiety on the five-membered ring in a spirocyclic manner, and CNX, bearing long triethylenegrycol (TEG) chains on the phenyl groups, show even stronger negative S_{TDM}. The results indicate that S_{TDM} of phosphole oxide dyes is sensitive to the substituents on their π-conjugated framework, giving rise to fine tuning of S_{TDM} even by a small structural modification.

Analysis by the molecular surface shape of dyes in NLCs. To elucidate the relation between the observed fluorescence anisotropy and the molecular structures of the dye, the order parameters of TDMs of fluorescence S_{TDM} were simulated using the molecular shapes and TDM directions on the molecular framework, both of which were calculated using QC methods (see previous sections on theoretical arguments and Methods for details). The estimated values are shown in Fig. 2 with the experiments for their comparison. Since the absolute values of S_{TDM} depend on undetermined ε (Supplementary Figure 3), only their semi-quantitative comparisons are justified with the feasible value $\varepsilon = 0.03\backslash$Å^{-2}. Nevertheless, an overall tendency of molecule-dependent S_{TDM} of experiments, high positive values for C5T and PMN, and lower values with both signs for phosphole oxide-based dyes is well reproduced by simulation. Focusing on the components of S_{TDM} (Eq. (1)), it is possible to discuss how the anisotropy of molecular shapes and TDM directions affect

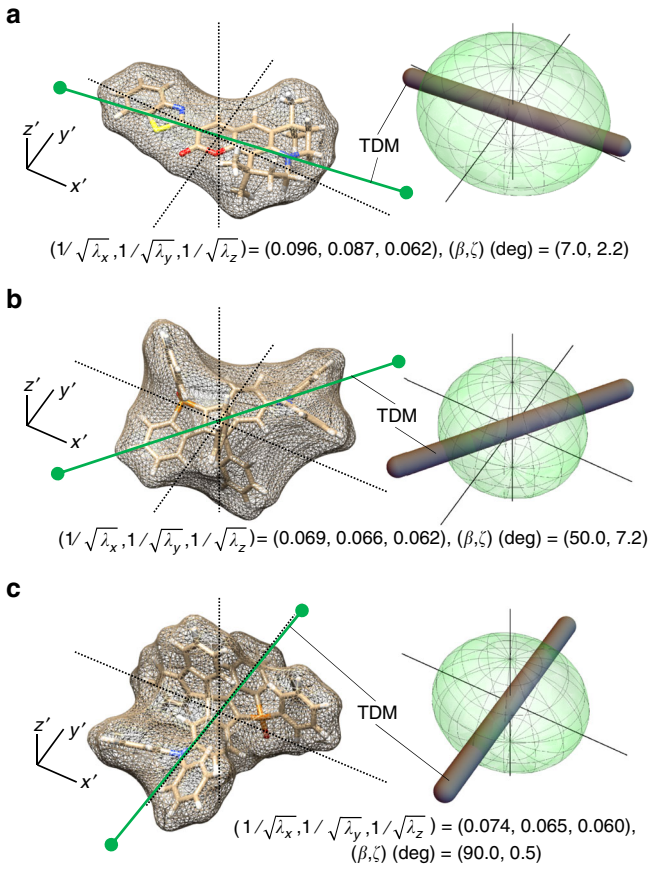

Fig. 3 Optimised molecular structures and surface tensor ellipsoids with TDM vectors. Optimised structures of (**a**) C5T, (**b**) CBX and (**c**) CBF on the molecular coordinate with the *x*′-, *y*′ and *z*′-axes chosen as the long, middle and short axes of the corresponding tensor ellipsoids shown on the right, respectively. The radii are also shown. Here, the configurations with the TDM vector $\boldsymbol{\mu}$ in the octant with $0 \le \mu_x$, $0 \le \mu_y$ and $0 \le \mu_z$, ie, $0 \le \zeta \le \frac{\pi}{2}$, are chosen as representatives. Note that other configurations allowed under the three mirror symmetries with respect to the *x*′*z*′, *x*′*y*′ and *y*′*z*′ planes are equally realised. Although the phosphole oxide-based dyes have chiral centres, the experimentally used racemic mixtures cover all configurations considered. The meshes covering molecules indicate the molecular surfaces. See Supplementary Figures 4 and 5 for corresponding data of other dyes and those of absorption, respectively

S_{TDM} and the possible reasons for some discrepancies in the tendency as follows.

Figure 3 and Supplementary Figure 4 show optimised geometries and surface tensor ellipsoids (with values of radii) with TDM vectors (with values of polar angles) of S_1 states on the molecular framework. The TDM vectors of phosphole oxide-based dyes lay on the π-conjugated plane. The eigenvalues obtained by diagonalizing the surface tensor matrix **Q** shown in Supplementary Table 2 were used to determine the LX direction, which corresponds to the *x*'-axis on the molecular coordinate.

Anisotropy of the molecular shape can be recognised visually from the shape of the tensor ellipsoid and quantitatively from λ_S and λ_D defined by Eq. (3), and shown in Fig. 4, where the larger λ_S or λ_D means higher uniaxiality or flatness of molecules, respectively. The results show that C5T, PMN, CBF and CNX exhibit higher uniaxiality and C5T exhibits higher flatness. Since these characters of molecular shapes have been incorporated into **S** through Eqs. (4)–(9), the molecule-dependent values of λ_S or λ_D show a similar tendency of S_{LX} or D_{LX} (Eqs. (10), (11)), respectively (Fig. 4). Apparently, the higher uniaxiality of the molecular shape leads to a higher uniaxial order parameter S_{LX}, ie, the narrower distribution of γ around 0.

The observable fluorescence light is emitted from the TDM fixed on the molecular framework with the angles (β,ζ). Since the molecular framework, ie, molecular coordinate, fluctuates on the laboratory coordinate, which is completely characterised by S_{LX} or D_{LX}, the observable S_{TMD} has forms of products $S_{LX}S_\beta$ and $D_{LX}D_{\beta\zeta}$ (Eq. (1)). Note that the effect of $D_{LX}D_{\beta\zeta}$ on S_{TMD} is 1/3 that of $S_{LX}S_\beta$. Although this term may have non-negligible contribution in general, on the present dyes, $\frac{1}{3}D_{LX}D_{\beta\zeta}$ appear small; S_{TDM} is mainly governed and explained by the $S_{LX}S_\beta$ term (Fig. 4). Noting $S_{LX} \ge 0$ by definition, the sign of S_{TDM} is practically determined by that of S_β.

C5T, PMN and CBM show high values of S_β close to one (Fig. 4), indicating that the TDM is almost parallel to the LX (Fig. 3a, Supplementary Figure 4b and 4e). Owing to the relatively higher S_{LX} of C5T and PMN mainly originating from their elongated shape, their S_{TDM} also result in higher values. On the other hand, CBM shows a smaller S_{LX}, giving a lower S_{TDM}. Both S_{LX} and S_β of CP2 and CBX are small, also resulting in lower S_{TDM}. In other words, the lower S_{TDM} for CBM, CP2 and CBX are attributed to their molecular shapes with low uniaxiality λ_S. The negative values of S_β and the relatively higher values of S_{LX} for CBF and CNX result in the conspicuous negative S_{TDM}. This originates from the rigid planar geometry of the spirocyclic fluorene moiety perpendicular to the π-conjugated plane for CBF (Fig. 3c) and long TEG chains connected to two phenyl groups protruding from the CNX plane (Supplementary Figure 4g).

The main discrepancy of the calculated S_{TDM} from experimental ones is found on CP2, CBM and CBX, which show lower S_{TDM}, as stated above. Since the differences between their eigenvalues $\left(\lambda_x, \lambda_y, \lambda_z\right)$ (Supplementary Table 2) are relatively small, the eigenvector directions, ie, the LX direction, become sensitive to the small errors in the calculated molecular shape through the surface tensor **Q**. Indeed, the current analyses of molecular surfaces rely on the particular optimised geometries without considering the conformational flexibility of substituents, such as phenyl groups and NPh_2 group on the π-conjugated plane. A similar reason should be also responsible for the discrepancy found in CNX, which has flexible TEG chains. Since the TEG chains have been considered rigid in the present calculation, the molecular uniaxiality should be overestimated, resulting in higher λ_S and S_{LX}, and thus, giving highly negative S_{TDM} with negative S_β. These discrepancies suggest the limitation on the accuracy of the present molecular-shape-based estimation of molecular alignment in NLCs; the difficulties may occur in the cases of molecules with low-molecular uniaxiality or high internal flexibility.

The current analytical method of the dye alignment in NLCs based on the molecular shapes and TDM vectors to the fluorescence anisotropy is also applicable to the results of absorption anisotropy (Supplementary Figures 2, 5 and 6). The slight differences between absorption and fluorescence anisotropy, which was already noted above, are also qualitatively reproduced small differences in the optimised molecular geometries at ground S_0 and excited S_1 states by this method.

Moreover, the careful inspection of the optimised geometries in the S_0 and S_1 states gave insights into the difference in the internal molecular flexibility that affects the effective molecular shape and is not unfortunately considered in the present analysis. As a model case, we selected CBF, which exhibits the highest positive S_{TDM} and $S_{TDM-Abs}$ values (Supplementary Figure 7). The bond lengths in the π-conjugated frameworks in the S_1 state revealed significant difference to those in the S_0 state with an increased quinoidal character. For instance, the C–C bonds *f*, *h* and *j* were elongated by 0.033, 0.074 and 0.026 Å, respectively, while the C–C bonds *g*, *i*, and

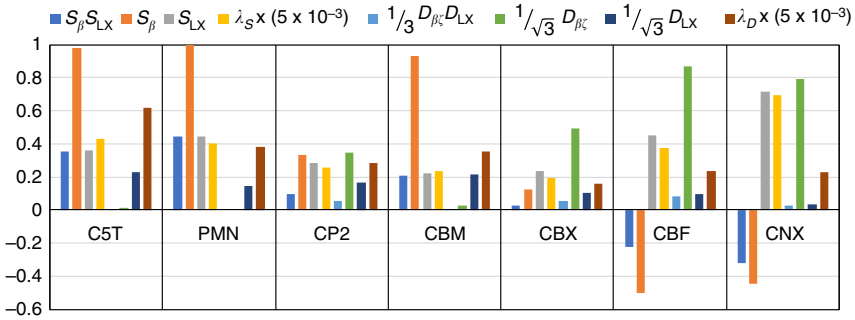

Fig. 4 Estimated components of order parameters from molecular shape analysis. The components of $S_{TDM-calc} = S_\beta S_{LX} + 1/3 D_{\beta\zeta} D_{LX}$ and anisotropy indices of the molecular shape, λ_S and λ_D (Å^2). Theoretically, S_{LX} and D_{LX} are closely correlated to λ_S and λ_D, respectively. Note that $0 \le S_{LX}$ and $0 \le S_{LX}$ according to the present choice of the molecular coordinate, and thus, the signs of $S_\beta S_{LX}$ and $1/3 D_{\beta\zeta} D_{LX}$ are determined by S_β and $D_{\beta\zeta}$, respectively. See Supplementary Figure 6 for corresponding data for absorption

C–N bond *p* were shortened by 0.059, 0.049 and 0.020 Å, respectively. The degree of bond alternation in the fused benzene rings also increased slightly. Moreover, the torsion angle between π-conjugated plane and the terminal NPh_2 group, defined by the dihedral angle of C15–C14–N17–C20, decreased from 37.68° to 33.25°. These results clearly demonstrate that the bond order of C14–N17 bond between π-conjugated plane and the terminal NPh_2 group significantly increased in the S_1 state, indicative of the higher rotational barrier in the S_1 state with respect to the S_0 state. In the other words, these results indicate that the discrepancy between the simulated and experimental values of λ_S and S_{LX} in the S_1 state should be smaller than those in the S_0 state, since the error on the estimation of the effective anisotropy of the molecular shape should be smaller owing to the suppression of internal rotation of the terminal NPh_2 group in the S_1 state. This can be a reason for the lower $|S_{TDM}|$ on absorption than that on fluorescence, which has been found experimentally for CBX and CBF. Although the effective molecular flatness (λ_D and D_{LX}) should also depend on the internal rotational degree, the effect is rather complex to be discussed even qualitatively and would be highly molecule-dependent.

Nevertheless, with caution to the property, the present model is still useful to understand the relation between molecular shapes and alignment in anisotropic phase. In the present phosphole oxide-based dyes, with increasing number, size and rigidity of substituents protruded from the π-conjugated plane, on which TDM lays, the LX tends to deviate from the TDM with angle β over the magic angle, ~54.7°, showing controllability of the fluorescence anisotropy from positive to negative property. Moreover, although it is difficult to predict in advance, the fine tuning of S_{TDM} are expected by tuning the substituents.

Note that the present phosphole oxide-based dyes are always associated with one phenyl group that is bonded to the phosphorus and protrudes from the π-conjugated plane. Since the phenyl group may also play a role in causing deviation of the LX from the TDM laying on the π-conjugated plane, it is beneficial to evaluate the effect. Here, with the aid of the present theoretical analysis, an analysis has been conducted on a trial compound (CBF-S) analogue to CBF (Supplementary Figure 8), on which the *P*-phenylphosphine oxide (>P(=O)Ph) is replaced with sulphone (>SO_2) removing the phenyl group of interest. The calculated S_{TDM} for fluorescence shows a low positive value of ~0.14 (Supplementary Figure 8b), indicating, as expected, that the phenyl group is also important to tilt the LX from the TDM laying on the π-conjugated plane, which has been observed for CBF and CNX. The components of S_{TDM} also suggest that CBF-S has lower anisotropy in its shape (low λ_S and S_{LX} ~0.23), which is the main reason for the low S_{TDM}, similarly to the cases found on CP2 and CBM. Originally, the phenyl group attached to the phosphorus has been designed and required because of the synthetic reason, ie, availability of the starting materials and the stability toward the reaction conditions[39,47,48]. Here it is theoretically suggested that the structural nature, ie, >P(=O)Ph, also plays an important role in realising negative fluorescence anisotropy of phosphole oxide-based dyes in the present NLCs.

Discussion

As outlined in the Results section, in general, $D_{LX} D_{\beta\zeta}$ may contribute to S_{TDM} (Eq. (1)), which, however, has not been the case for the dyes evaluated here. It is profitable to mention the general guiding principle on the molecular design of dyes in terms of the molecular shape and the TDM direction in the molecular framework for controlling the fluorescence anisotropy. To obtain highly positive fluorescence anisotropy, both S_{LX} and S_β should be high, which means that an elongated uniaxial shape with the TDM parallel to the LX is preferred. This strategy has already been well known through the active studies on the guest–host mode[28–34].

Beyond this, in some FOM studies of anisotropic media, isotropic fluorescence may be useful to image the concentration distribution of dyes in the anisotropic medium rather than the anisotropic medium. Such dyes can be called 'phoney dyes'[52]. In this case, spherical shapes, which reduce S_{LX} and D_{LX}, are required and/or the TDM should have (β,ζ) close to (~54.7°, 45°).

To obtain highly negative fluorescence anisotropy useful in FPOM, S_{LX} and $-S_\beta$ should be high, which means that the elongated uniaxial shape with the TDM perpendicular to the LX is preferred. Moreover, a higher D_{LX}, ie, molecular flatness, with ζ~90° further improves the negative anisotropy. By designing the structures of dye molecules in terms of the whole molecular shape and TDM orientation under the present principle, the finer optimisation of the fluorescence anisotropy would be possible.

In summary, we evaluated a series of phosphole oxide-based dyes and found that their fluorescence anisotropy varies from positive to negative as the number, size and rigidity of aromatic substituents protruding from the π-conjugated plane increase. The present series of phosphole oxide dyes shows gradual change in fluorescence anisotropy ranging from negative to positive values owing to subtle structural substitutions and may provide fluorescent probes useful in the FOM studies of anisotropic medium[40]. Our analysis based on molecular shape provides support to understand the relation between the molecular structure and the observed fluorescence anisotropy. This suggests that the precise control of fluorescence anisotropy is possible by the molecular design considering their statistical alignment states, which will be useful in FPOM studies of NLCs and other anisotropic media.

Methods

Materials. 4-Cyano-4′-pentylbiphenyl (5CB) and *N*-(4-methoxybenzyidene)-4-butylaniline (MBBA) were purchased from Tokyo Chemical Industry. 4,4′-Dibutyl and 4,4′-dihexyl derivatives of diphenyldiacetylene[53] were synthesised using a modified procedure[54] to prepare a 1:1 (molar) mixture of the diphenyldiacetylene derivatives. Since each derivative has a linear 'phenyl–triple bond–triple bond–phenyl' structure, the mixture is referred as PTTP here. The nematic temperature range of PTTP was examined using a polarised optical microscope (BX-51P, Olympus) with a temperature-controlled stage (INSTEC, mk 1000). 5CB, MBBA and PTTP were used as room-temperature NLCs with different permanent dipole moments and directions with respect to the nematic director. The nematic temperature range, relative permeability, permanent dipole moment and the angle to the nematic director for the NLCs are as follows: 22–35 °C; +10; 5D; 0° for 5CB[55], 20–47 °C; −5; 2–4D; 60° for MBBA[55], and 28–93 °C; +1; very small; N/A for PTTP[53]. The chemical structures of these NLCs are shown in Supplementary Figure 9.

Two reference dyes coumarin 545T (C5T)[56] and pyrromethene 597 (PMN, (((4-*tert*-Butyl-3,5-dimethyl-1*H*-pyrrol-2-yl)(4-*tert*-butyl-3,5-dimethyl-2*H*-pyrrol-2-ylidene)methyl)methane)(difluoroborane))[57] were purchased from Tokyo Chemical Industry. Five phosphole oxide-based fluorescent dyes (racemic mixtures)—(CP2), (CBM), (CBX), (CBF) and (CNX) (Fig. 2b)—were synthesised according to previously reported methods[39,46–48].

Preparation of planar LC cells. For measurements of fluorescence dichroic properties, a planar cell with unidirectional planar alignment (KSRP-02/A111P1NSS05, EHC; cell gap of 2 ± 0.5 μm) filled with NLCs doped with dyes (0.1 wt%) was used. For measurements of absorption dichroic properties, a planar cell with a thicker gap of unidirectional planar alignment (KSRP-50/A111P1NSS05, EHC; cell gap of 50 ± 2.5 μm) filled with NLCs doped with dyes (0.1 wt%) was used to gain the absorption intensity. The alignment surfaces of the planar cells were uniaxially rubbed polyimide (LX-1400, Hitachi-Kasei) coatings.

Optical microscopy for anisotropy evaluation. After we confirmed the LC alignment direction, ***n***, of the LC cells using POM, the fluorescence anisotropy was evaluated using a conventional FOM, where the light source was mounted above the sample and the excitation light was passed through the microscope objective lens on its way toward the sample. A Xe lamp (75 W) was used as the light source. To collect the fluorescence emission from dyes, we used a fluorescence filter set (U-MWIB-3, Olympus) comprising an excitation filter that transmitted light with wavelengths between 460 and 495 nm and an emission filter that transmitted light with wavelength larger than 510 nm. The dyes were excited with natural (unpolarised) light and the emission intensity $I_{\parallel}$ or $I_{\perp}$ was measured through a polariser with the direction parallel or perpendicular to ***n***, respectively. All dyes used in the present study could be excited and emit detectable fluorescence with the fluorescence filter set (see Supplementary Table 1 for typical peaks of absorption and emission from the literature). Since the long-wavelength edge of the absorption band was excited, the excitation and emission of all dyes were assigned to the transition between ground S_0 and excited S_1 states. The fluorescence emission was collected using a Nikon DS-Ri2 CMOS camera with a high linearity (>5%) between the input light intensity and detected power connected to a computer and controlled through imaging software (NIS-Elements, Nikon). An objective lens with a low numerical aperture (NA) of 0.15 (MPlanFLN 5×, Olympus) was used to reduce the effect of depolarisation due to NA[58]. It was also confirmed using different objective lenses that the effect of NA with some higher values, 0.25 and 0.50, on the fluorescence anisotropy results was negligible (Supplementary Figure 10), justifying the use of the microscope for the present evaluation.

To evaluate the absorption anisotropy, the transmitted light intensity $T_{\parallel}$ or $T_{\perp}$with the same range of the excitation band used for fluorescence measurements was collected through a polariser with the direction parallel or perpendicular to ***n***, respectively. The dichroic ratio for the absorption was calculated as $R_a = \log\left(T_{\parallel}/T_0\right)/\log(T_{\perp}/T_0)$, where T_0 is the blank transmitted intensity.

All measurements of fluorescence and absorption of dye-doped 5CB and MBBA were conducted at 23 °C. For the dye-doped PTTP, the measurements were conducted at 29 °C using the temperature-controlled stage.

QC calculations. All QC calculations were carried out using Gaussian 16 Revision A.03 suite of programs (Frisch, M. J. et al., *Gaussian 16 Revision A 03* (2016), Gaussian Inc., Wallingford CT) with default thresholds and algorithms. The geometry optimisations both in the ground state (S_0) and the first excited singlet state (S_1) and the TDM for the Frank–Condon vertical excitations between them were conducted using density functional theory (DFT) and time-dependent DFT with the Truhlar's M06-2X functional[59]. The basis sets employed in this study are aug-cc-pVDZ[60,61] for P, N and O and cc-pVDZ[61] for C and H. Stationary points for S_0 were optimised without any symmetry assumptions and confirmed by frequency analysis at the same level of theory.

Molecular shape analysis. To calculate the surface second-order tensor **T** (Eq. (2)), the molecular surfaces of the dyes were first constructed from the geometry optimised by QC calculations using the Michel Sanner's Molecular Surface[62] algorithm to define a solvent-excluded surface, using a probe radius of 3 Å and tessellating it into discrete surface elements at a density of ~5 vertices per Å^2, consistent with the previously reported studies[41–43]. The *i*th triangle mesh had a unit normal vector $\boldsymbol{t}_i$ and an area of s_i. Practically, **T** was calculated through the form of summation, $\mathbf{T} = \sum_{i=1}^{m}(\boldsymbol{t}_i \otimes \boldsymbol{t}_i)s_i$, where m is the total number of meshes. After diagonalization of **T**, axes (x', y', z') of the molecular coordinate were chosen as the eigenvectors with the corresponding eigenvalues $\left(\lambda_x, \lambda_y, \lambda_z\right)$ for x', y' and z' chosen as $\lambda_x \le \lambda_y \le \lambda_z$. To intuitively capture the molecular anisotropy, the tensor ellipsoid for each molecule on the molecular coordinate was illustrated through the equation $\lambda_x x^2 + \lambda_y y^2 + \lambda_z z^2 = 1$, where the ellipsoid had the longest length in the x'-axis. The corresponding TDM vector was also overlaid on the ellipsoid. The eigenvalues were also used to estimate the second-order tensor-order parameter **Q** of the dye molecule, ie, the order parameter of TDM, S_{TDM} through Eq. (1), as explained in the theoretical arguments in Results section. Although, to be exact, the interaction parameter ε in Eq. (3) should depend on the combination of the dye and NLC, temperature, and so on, it was chosen to be 0.03 Å^{-2} for all dyes as a first approximation, which was consistent with the value range reported previously[41].

Data availability. Data that support the findings of this study are available from the corresponding author upon reasonable request.

Received: 8 July 2018 Accepted: 13 August 2018
Published online: 03 September 2018

References

1. de Gennes, P. G. & Prost, J. *Physics of Liquid Crystals* (Clarendon, Oxford, 1993).
2. Vertogen, G. & de-Jeu, W. H. *Thermotropic Liquid Crystals, Fundamentals* (Springer-Verlag, Berlin, Heidelberg, 1988).
3. Kleman, M. & Lavrentovich, O. D. *Soft Matter Physics: An Introduction* (Springer-Verlag, New York, 2003).
4. Oswald, P. & Pieranski, P. *Nematic and Cholesteric Liquid Crystals* (Taylor & Francis, New York, 2005).
5. Singer, S. J. & Nicolson, G. L. Fluid mosaic model of structure of cell-membranes. *Science* **175**, 720–731 (1972).
6. Axelrod, D. Carbocyanine dye orientation in red cell membrane studied by microscopic fluorescence polarization. *Biophys. J.* **26**, 557–573 (1979).
7. Inoué, S., Shimomura, O., Goda, M., Shribak, M. & Tran, P. T. Fluorescence polarization of green fluorescence protein. *Proc. Natl Acad. Sci. USA* **99**, 4272–4277 (2002).
8. Jameson, D. M. & Ross, J. A. Fluorescence polarization/anisotropy in diagnostics and imaging. *Chem. Rev.* **110**, 2685–2708 (2010).
9. Lakowicz, J. R. *Principles of Fluorescence Spectroscopy* 3rd edn (Springer-Verlag: New York, 2006).
10. Valeur, B. & Berberan-Santos, M. N. *Molecular Fluorescence: Principles and Applications* (Wiley-VCH, Weinheim, 2013).
11. Lavrentovich, O. D. Topological defects in dispersed words and worlds around liquid crystals, or liquid crystal drops. *Liq. Cryst.* **16**, 117–124 (1998).
12. Poulin, P., Stark, H., Lubensky, T. C. & Weitz, D. A. Novel colloidal interactions in anisotropic fluids. *Science* **275**, 1770–1773 (1997).
13. Fleury, J.-B., Pires, D. & Galerne, Y. Self-connected 3D architecture of microwires. *Phys. Rev. Lett.* **103**, 267801 (2009).
14. Tkalec, U., Ravnik, M., Čopar, S., Žumer, S. & Muševič, I. Reconfigurable knots and links in chiral nematic colloids. *Science* **333**, 62–65 (2011).
15. Ravnik, M., Alexander, G. P., Yeomans, J. M. & Žumer, S. Three-dimensional colloidal crystals in liquid crystalline blue phases. *Proc. Natl Acad. Sci. USA* **108**, 5188–5192 (2011).
16. Ohzono, T. & Fukuda, J. Zigzag line defects and manipulation of colloids in a nematic liquid crystal in microwrinkle grooves. *Nat. Commun.* **3**, 701 (2012).
17. Sengupta, A., Bahr, C. & Herminghaus, S. Topological microfluidics for flexible micro-cargo concepts. *Soft Matter* **9**, 7251–7262 (2013).
18. Yoshida, H., Asakura, K., Fukuda, J. & Ozaki, M. Three-dimensional positioning and control of colloidal objects utilizing engineered liquid crystalline defect networks. *Nat. Commun.* **6**, 7180 (2015).
19. Higashiguchi, K., Yasui, K., Ozawa, M., Odoi, K. & Kikuchi, H. Spatial distribution control of polymer nanoparticles by liquid crystal disclinations. *Polym. J.* **44**, 632–638 (2012).
20. Wang, X., Miller, D. S., Bukusoglu, E., de Pablo, J. J. & Abbott, N. L. Topological defects in liquid crystals as templates for molecular self-assembly. *Nat. Mater.* **15**, 106–112 (2016).
21. Wang, X. et al. Experimental insights into the nanostructure of the cores of topological defects in liquid crystals. *Phys. Rev. Lett.* **116**, 147801 (2016).
22. Ohzono, T., Katoh, K. & Fukuda, J. Fluorescence microscopy reveals molecular localisation at line defects in nematic liquid crystals. *Sci. Rep.* **6**, 36477 (2016).

23. Fukuda, J. Do small molecules assemble at topological defects of a liquid crystal? *Proc. SPIE* **10125**, 1–7 (2017). 101250C.
24. Smalyukh, I. I., Shiyanovskii, S. V. & Lavrentovich, O. D. Three-dimensional imaging of orientational order by fluorescence confocal polarizing microscopy. *Chem. Phys. Lett.* **366**, 88–96 (2001).
25. Trivedi, R. P., Klevets, I. I., Senyuk, B., Lee, T. & Smalyukh, I. I. Reconfigurable interactions and three-dimensional patterning of colloidal particles and defects in lamellar soft media. *Proc. Natl Acad. Sci. USA* **109**, 4744–4749 (2012).
26. Trivedi, R. P. & Smalyukh, I. I. in *Fluids, Colloids and Soft Materials: An Introduction to Soft Matter Physics* 165–184 (eds Fernandez-Nieves, A. & Puertas, A. M.) Ch. 10 (Wiley, Berlin, 2016).
27. Zocher, H. On the polarisation of the fluorescence of dyestuffs dissolved in meso-phases. *Trans. Faraday Soc.* **35**, 34–37 (1939).
28. Heilmeier, G. H. & Zanoni, L. A. Guest-host interactions in nematic liquid crystals, a new electro-optic effect. *Appl. Phys. Lett.* **13**, 91–92 (1968).
29. Baur, G., Stieb, A. & Meier, G. Polarized fluorescence of dyes oriented in room temperature nematic liquid crystals. *Mol. Cryst. Liq. Cryst.* **22**, 261–269 (1973).
30. Osman, M. A., Pietronero, L., Scheffer, T. J. & Zeller, H. R. The dichroic ratio of pleochroic dyes dissolved in nematic liquid crystals. *J. Chem. Phys.* **74**, 5377 (1981).
31. Uchida, T. & Wada, M. Guest-host type liquid crystal displays. *Mol. Cryst. Liq. Cryst.* **63**, 19–43 (1981).
32. Bauman, D. The study of the guest effect on the nematic phase stabilization. *Mol. Cryst. Liq. Cryst.* **159**, 197–218 (1988).
33. Ivashchenko, A. V. *Dichroic Dyes for Liquid Crystal Displays* (CRC Press, Boca Raton, 1994).
34. Leslie, T. M., Goodby, J. W. & Filas, R. W. in *Liquid Crystals and Ordered Fluids* Vol. 4, 43–55 (eds Griffin, A. C. & Johnson, J. E.) (Plenum, New York, 1982).
35. Imazeki, S., Kaneko, M., Ozawa, T. & Mukoh, A. Anthraquinone dyes with negative dichroism. *Mol. Cryst. Liq. Cryst.* **151**, 219–231 (1988).
36. Chigrinov, V., Prudnikova, E., Ng, K. W. & Kwok, H. S. Non polarizer guest-host mode based on dyes with negative dichroism. *Jpn. J. Appl. Phys.* **42**, 1297–1300 (2003).
37. Debije, M. G., Menelaou, C., Herz, L. M. & Schenning, A. P. H. J. Combining positive and negative dichroic fluorophores for advanced light management in luminescent solar concentrators. *Adv. Opt. Mater.* **2**, 687–693 (2014).
38. Grabchev, I., Mykowskaa, E., Moneva, I. & Bauman, D. Molecular orientation of some fluorescent dichroic dyes in nematic liquid crystal. *Z. Naturforsch.* **59**, 368–374 (2004).
39. Wang, C. et al. A phosphole oxide based fluorescent dye with exceptional resistance to photobleaching: a practical tool for continuous imaging in STED microscopy. *Angew. Chem. Int. Ed. Engl.* **54**, 15213–15217 (2015).
40. Ohzono, T. et al. Uncovering different states of topological defects in schlieren textures of a nematic liquid crystal. *Sci. Rep.* **7**, 16814 (2017).
41. Ferrarini, A., Moro, G. J., Nordio, P. L. & Luckhurst, G. R. A shape model for molecular ordering in nematics. *Mol. Phys.* **77**, 1–15 (1992).
42. Ferrarini, A., Janssen, F., Moro, G. J. & Nordio, P. L. Molecular surface and order parameters in liquid crystals. *Liq. Cryst.* **26**, 201–210 (1999).
43. Di-Matteo, A., Ferrarini, A. & Moro, G. J. Effects of electrostatic interactions on orientational order of solutes in liquid crystals. *J. Phys. Chem. B* **104**, 7764–7773 (2000).
44. Kamberaj, H., Low, R. J. & Neal, M. P. Correlation between molecular chirality and helical twisting power: a computer simulation study. *Mol. Phys.* **104**, 335–357 (2006).
45. Sims, M. T., Abbott, L. C., Cowling, S. J., Goodby, J. W. & Moore, J. N. Principal molecular axis and transition dipole moment orientations in liquid crystal systems: n assessment based on studies of guest athraquinone dyes in a nematic host. *Phys. Chem. Chem. Phys.* **19**, 813–827 (2017).
46. Wang, C. et al. Super-photostable phosphole-based dye for multiple-acquisition stimulated emission depletion imaging. *J. Am. Chem. Soc.* **139**, 10374–10381 (2017).
47. Adler, R. A., Wang, C., Fukazawa, A. & Yamaguchi, S. Tuning the photophysical properties of photostable benzo[*b*]phosphole P-oxide-based fluorophores. *Inorg. Chem.* **56**, 8718–8725 (2017).
48. Yamaguchi, S., Fukazawa, A. & Taki, M. Phosphole P-oxide-containing π −electron materials: synthesis and applications in fluorescence imaging. *J. Synth. Org. Chem. Jpn.* **75**, 1179–1187 (2017).
49. van der Est, A. J., Kok, M. Y. & Burnell, E. E. Size and shape effects on the orientation of rigid molecules in nematic liquid crystals. *Mol. Phys.* **60**, 397–413 (1987).
50. Zimmerman, D. S. & Burnell, E. E. Size and shape effects on the orientation of solutes in nematic liquid crystals. *Mol. Phys.* **69**, 1059–1071 (1990).
51. Zimmerman, D. S. & Burnell, E. E. Anisotropic short range potentials for solutes in nematic liquid crystals. *Mol. Phys.* **78**, 687–702 (1993).
52. Bahadur, B. in *Handbook of Liquid Crystals* (eds Demus, D., Goodby, J. W., Gray, G. W., Spiess, H. W. & Vill, V.) Vol. 2A, 257–302 (Wiley-VHC, Weinheim, 1998).
53. Wu, S.-T. et al. Room-temperature diphenyl-diacetylene liquid crystals. *Appl. Phys. Lett.* **61**, 630–632 (1992).
54. Arakawa, Y. et al. Synthesis of diphenyl-diacetylene-based nematic liquid crystals and their high birefringence properties. *J. Mater. Chem.* **22**, 8394–8398 (2012).
55. Barnik, M. I., Blinov, L. M., Dorozhkin, A. M. & Sthykov, N. M. Second optical harmonic generation induced by an electric field in liquid crystals with dielectric anisotropy of opposite signs. *Zh. Eksp. Teor. Fiz.* **84**, 582–585 (1983).
56. Chen, C. H. & Tang, C. W. Efficient green organic light-emitting diodes with sterically hindered coumarin dopants. *Appl. Phys. Lett.* **79**, 3711–3713 (2001).
57. Prieto, J. B., Arbeloa, F. L., Martınez, V. M., López, T. A. & Arbeloa, I. L. Photophysical properties of the pyrromethene 597 dye: solvent effect. *J. Phys. Chem. A* **108**, 5503–5508 (2004).
58. Fisz, J. J. Fluorescence polarization spectroscopy at combined high-aperture excitation and detection: application to one-photon-excitation fluorescence microscopy. *J. Phys. Chem. A* **111**, 8606–8621 (2007).
59. Zhao, Y. & Truhlar, D. G. The M06 suite of density functionals for main group thermochemistry, thermochemical kinetics, noncovalent interactions, excited states, and transition elements: two new functionals and systematic testing of four M06 functionals and 12 other functional. *Theor. Chem. Acc.* **120**, 215–241 (2008).
60. Kendall, R. A., Dunning, T. H. Jr. & Harrison, R. J. Electron affinities of the first-row atoms revisited. Systematic basis sets and wave functions. *J. Chem. Phys.* **96**, 6796 (1992).
61. Woon, D. E. & Dunning, T. H. Jr. Gaussian basis sets for use in correlated molecular calculations. III. The atom aluminum through argon. *J. Chem. Phys.* **98**, 1358 (1993).
62. Sanner, M. F., Olson, A. J. & Spehner, J. C. Reduced surface: an efficient way to compute molecular surfaces. *Biopolymers* **38**, 305–320 (1996).

Acknowledgements

The authors would like to thank Y. Norikane, G. Watanabe, R. Yamaguchi and T. Uchida for useful discussions. T.O. and A.F. were supported by a grant for promotion of cooperation between Nagoya University and AIST.

Author contributions

T.O. conceived the central idea, performed the experiments and molecular surface analysis, and analysed the results. A.F. carried out the QC calculations. T.O. and A.F. contributed to experimental designs, theoretical arguments and writing the manuscript. C.W., A.F. and S.Y. designed and synthesised phosphole oxide-based dyes. T.Y. synthesised components of the non-polar NLC (PTTP). All authors discussed the results and manuscript.

Additional information

Supplementary information accompanies this paper at https://doi.org/10.1038/s42004-018-0055-6.

Competing interests: The authors declare no competing interests.

Reprints and permission information is available online at http://npg.nature.com/reprintsandpermissions/

Publisher's note: Springer Nature remains neutral with regard to jurisdictional claims in published maps and institutional affiliations.